Modeling of Knudsen layer effects in micro/nano scale gas flows

Nishanth Dongari
Department of Mechanical Engineering
University of Strathclyde
Glasgow G1 1XJ, UK
Email: nishanth.dongari@strath.ac.uk

Yonghao Zhang
Department of Mechanical Engineering
University of Strathclyde
Glasgow G1 1XJ, UK
Email: yonghao.zhang@strath.ac.uk

Jason M Reese
Department of Mechanical Engineering
University of Strathclyde
Glasgow G1 1XJ, UK
Email: jason.reese@strath.ac.uk

We propose a power-law based effective mean free path (MFP) model, so that the Navier-Stokes-Fourier equations can be employed for the transition-regime flows typical of gas micro/nano devices. The effective MFP model is derived for a system with planar wall confinement by taking into account the boundary limiting effects on the molecular free paths. Our model is validated against molecular dynamics simulation data and compared with other theoretical models. As gas transport properties can be related to the mean free path through kinetic theory, the Navier-Stokes-Fourier constitutive relations are then modified in order to better capture the flow behaviour in the Knudsen layers close to surfaces. Our model is applied to fully developed isothermal pressure-driven (Poiseuille) and thermal creep gas flows in micro-channels. The results show that our approach greatly improves the near-wall accuracy of the Navier-Stokes-Fourier equations, well beyond the slip-flow regime.

1 Introduction

In micro/nano scale gas flows, the small system dimensions mean that the non-dimensional Knudsen number, Kn, defined as the ratio of the molecular mean free path (MFP) of the gas, λ, to a characteristic flow field dimension, indicates the flows are often rarefied. As Kn increases, the behaviour of a gas flow near a solid bounding surface is dominated by the effect of gas molecule-surface interactions. This leads to the formation of a Knudsen layer (KL): a local thermodynamically non-equilibrium region extending $\sim O(\lambda)$ from the surface. Fig. 1 is a schematic of the gas velocity profile in the KL in a shear-driven flow. Although the Navier-Stokes-Fourier (NSF) equations with classical velocity-slip and temperature-jump boundary conditions [1] can often adequately predict the flow field outside the KL, they fail to capture the non-equilibrium flow behavior of the KL itself [2].

In the KL, gas molecule-surface collisions are more frequent than gas molecule-molecule collisions, i.e. the gas MFP will effectively be reduced in the KL. It is well-known from the kinetic theory of gases that viscosity and thermal conductivity can be interpreted in terms of the collisions of gas molecules, and of the free paths of the molecules between collisions. Linear constitutive relations for shear stress and heat flux are no longer necessarily valid in the KL. Traditionally, kinetic methods, such as directly solving the Boltzmann equation [3] or the direct simulation Monte Carlo (DSMC) method [4], can offer more accurate descriptions of non-equilibrium flows. However, these methods are computationally expensive for low-speed flows in the slip- and transition-flow regimes, and not always practical for engineering design and simulation purposes.

Wall-distance scaling functions for the constitutive relationships for shear stress and heat flux have been proposed recently: Kn-dependent functions [5], and power-law scaling of constitutive relations [6–8] to extend the validity of hydrodynamic models to the transitional regime gas flows. This phenomenological observation of the bounding wall effect on the constitutive laws has been interpreted as the modification of the gas MFP due to gas molecule/wall surface collisions [9]. Guo *et al.* [10] implemented the effective MFP expression derived by Stops [11], in conjunction with a second-order slip boundary condition, and obtained good results for isothermal and non-isothermal pressure-driven rarefied gas flows when compared to conventional higher-order slip and jump models.

Stops' [11] geometry-dependent effective MFP, $\lambda_{\mathrm{eff(S)}}$, is defined as the average distance a gas molecule will travel between consecutive collisions with either another gas

molecule or the solid wall. Stops used the classical probability distribution function, $\psi(r) = \lambda^{-1} \exp(-r/\lambda)$ [12], for which the probability that a given gas molecule will travel a distance in the range r to $r+dr$ between two successive collisions is $\psi(r)dr$. If the gas is not bounded, the MFP of the gas molecule ensemble is simply $\int_0^\infty Nr\psi(r)dr/N = \lambda$, where N is the total number of molecules. If a solid bounding surface is included in the system, however, some molecules will hit the surface and their free flight paths will be terminated. The MFP of all the gas molecules in the system will therefore be smaller than λ, due to this boundary limiting effect. Recently, Arlemark *et al.* [13] developed a probability function-based effective MFP ($\lambda_{\mathrm{eff(A)}}$) expression, also using the classical exponential form of the distribution function. However, comparison of both of these effective MFP profiles [11, 13] with molecular dynamics (MD) simulation data [14, 15] shows that both models are useful only up to Knudsen numbers of about 0.2.

The MD simulation data [14] illuminates the limitations of the conventional exponential form of probability distribution function for gases in the transition regime. Stops [11] also pointed out that the exponential form of distribution function only provides an accurate description of a gas under thermodynamic equilibrium. While exponential probability distribution functions are fundamental models in many transport processes, they miss some features of transport in non-equilibrium systems [16]. This is evident in, e.g., the transport of tracer particles released in pressure-gradient-driven turbulence [17], transient photoconductivity experiments [18] and the dynamics of electrons due to Langmuir waves [19]. This has triggered a series of studies in which the Brownian paradigm was abandoned, and anomalous diffusive transport description proposed using Lévy and power-law (PL) probability distributions [14, 20]. Recently, Lockerby and Reese [8] proposed a PL scaling, based on the kinetic theoretical results of Sone [3], for the stress/strain-rate relationship in isothermal KLs. This provided more accurate results than conventional constitutive relationships with higher-order slip models.

In this paper, we hypothesize an effective MFP based on a PL probability distribution of the molecular free paths in a gas close to a planar wall. We show that this model captures some of the nonlinear trends associated with the physics of transition regime gas flows. Our PL-based effective MFP is validated against MD simulation data [14] up to $Kn = 2$, and also compared with the theoretical models of Stops [11] and Arlemark *et al.* [13]. Non-linear constitutive relationships are then developed through this new geometry-dependent effective MFP model. The resulting continuum equations, in conjunction with a second-order slip boundary condition, are then tested on both isothermal pressure-driven gas flows and thermal creep flows in micro/nano-channels. Results are compared with the solution of the Boltzmann equation, and DSMC and experimental data. The relative merits of this new constitutive scaling proposition are then discussed.

2 An Effective Molecular Mean Free Path

2.1 Theoretical development

Let us consider a group of similar gas molecules moving through a gas at a speed $\bar{v}$ and experiencing a collision rate of $\dot{\theta}_v$, where the molecular mean free path $\lambda = \bar{v}/\dot{\theta}_v$. The probability distribution of free paths can be expressed as [12]:

$$\psi(r) = \frac{1}{\lambda} \exp\left(-\frac{|r|}{\lambda}\right), \tag{1}$$

where $|r|$ is the length $\bar{v}t$ of free path that has been travelled at time t by each molecule. We can easily integrate Eq. 1 under thermodynamic equilibrium conditions. By *thermodynamic equilibrium* we mean that the probability of a certain microscopic state (such as $\dot{\theta}_v$) averaged over the details of the interactions, does not change in time or space [21]. So $\psi(r)$, the probability distribution of free paths, is only exponential under thermodynamic equilibrium conditions and when the gas is unbounded.

In a rarefied gas system, in which gas molecules may not suffer sufficiently frequent collisions with other gas molecules to attain equilibrium conditions, deviations from thermodynamic equilibrium may have substantial effects. It is certainly difficult to evaluate what the probability distribution function $\psi(r)$ is, as local fluctuations in $\dot{\theta}_v$ will be significant in non-equilibrium situations [14]. However, by means of appropriate physical arguments, we can hypothesize a distribution function that may be more appropriate for non-equilibrium conditions than the exponential one above [21].

Montroll & Scher [20] pointed out that a finite moment of the probability distribution function implies an exponential character of the randomness. So results obtained using exponential forms of the distribution functions are essentially the same as those for homogeneous media at equilibrium. A distribution function with diverging higher-order moments (such as the standard deviation) is essential to anomalous transport. In transient photoconductivity experiments, concentration distributions may have a long tail such that the standard deviation is diverging. This long-tail problem is common to various flows in non-uniform media, in many fields such as chemical engineering and environmental sciences [22].

Montroll & Scher [20] theoretically showed that anomalous electron transport is characteristic of a distribution function with diverging higher-order moments, in particular a power-law (PL) form of the distribution function. Second moments (i.e. standard deviation) diverge for the distribution functions describing the probability density distribution of electrons in photoconductivity experiments. However, the first moment also diverges in this case, whereas it should be finite in the gas flow case in order to achieve a finite MFP value.

We therefore hypothesize a PL form with diverging higher-order moments, for the probability distribution function for non-equilibrium gas MFP, instead of the classical exponential form of distribution function. Here we propose for investigation the following form of molecular free path

distribution function:

$$\psi(r) = C(a+r)^{-n}, \tag{2}$$

where a and C are constants with positive values that are determined through the zero and first moments. The range of values for the exponent n can be obtained by making one of the higher-order moments divergent. Zero and first moments are given as follows:

$$1 = \int_0^\infty C(a+r)^{-n} dr, \tag{3}$$

$$\lambda = \int_0^\infty Cr(a+r)^{-n} dr. \tag{4}$$

Equation 3 requires the probability to range only from zero to one. Equation 4 defines the unconfined, conventional MFP value, λ. It then follows that

$$C = (n-1)a^{n-1}, \tag{5}$$

$$a = \lambda(n-2). \tag{6}$$

The MFP for thermal cases is defined as $\lambda_T = 1.922\lambda_{\mathrm{HS}}$ [3], where the subscript HS denotes hard-sphere molecules. The modified constants for thermal cases are therefore:

$$C_T = (n-1)(a_T)^{n-1}, \tag{7}$$

$$a_T = \lambda_T(n-2). \tag{8}$$

If $n < 2$, then $a < 0$, and the distribution function is negative. The standard deviation (second moment) of the distribution function given by Eq. 2 diverges only for $n \leq 3$; so we must have $2 < n \leq 3$. If one wishes to make the i^{th} moment diverging, then $n_{max} = i+1$. For a finite n, the distribution function will have finite moments and describes a system deviating from equilibrium. Thus, n acts as a decisive parameter to define the extent of deviation from equilibrium. In the present paper, we test $n = 3$ unless otherwise explicitly stated.

The effective MFP expression developed by Stops [11], $\lambda_{\mathrm{eff(S)}}$, was derived using solid-angle-analysis. Here we use instead the approach of Arlemark *et al.* [13], based on an integrated form of the probability distribution function, i.e.

$$p(r) = \int_r^\infty \psi(r) dr = \left[1 - \left(1 + \frac{r}{a}\right)^{1-n}\right], \tag{9}$$

which describes the probability a gas molecule travels a distance r without experiencing a collision.

Our model is derived for the two-planar-wall configuration shown in Fig. 2. We use the notation r^- if a test molecule is traveling in the negative y-direction, and r^+ if the molecule is traveling in the positive y-direction. We also use the notations θ^- and θ^+ for the equally probable zenith angle traveling direction of the molecule. These quantities are related through $r^- = (H/2+y)/\cos\theta^-$ and $r^+ = (H/2-y)/\cos\theta^+$, where H is the distance between the two parallel plates.

The MFP based on the PL form of distribution function, $\lambda_{\mathrm{eff(PL)}}$, is expressed by weighting the unconfined MFP, λ, with $p(r)$ as follows:

$$\begin{aligned}\lambda_{\mathrm{eff(PL)}} &= \frac{\lambda}{2}\left[p(r^-) + p(r^+)\right] \\ &= \lambda\left\{1 - \frac{1}{2}\left[\left(1+\frac{r^-}{a}\right)^{1-n} + \left(1+\frac{r^+}{a}\right)^{1-n}\right]\right\}\end{aligned} \tag{10}$$

A 3-dimensional MFP depending on the gas molecule's distance to a surface is then obtained by averaging the free path with respect to θ^- and θ^+ in the range $[0, \pi/2]$ using the mean integral theorem,

$$< \lambda_{\mathrm{eff(PL)}}(\theta) >= \frac{2}{\pi}\int_0^{\pi/2} \lambda_{\mathrm{eff(PL)}}(\theta) d\theta, \tag{11}$$

where the integration domain is illustrated in Fig. 3 for a gas molecule travelling in the negative y-direction. Averaging over the free path in Eq. (11), using Simpson's numerical integration involving 16 subintervals, results in $\lambda_{\mathrm{eff(PL)}} = \lambda\beta_{\mathrm{PL}}$, where

$$\begin{aligned}\beta_{\mathrm{PL}} = 1 - \frac{1}{96}\Bigg[&\left(1+\frac{H/2-y}{a}\right)^{1-n} + \left(1+\frac{H/2+y}{a}\right)^{1-n} \\ &+ 4\sum_{i=1}^{8}\left(1+\frac{H/2-y}{a\cos[(2i-1)\pi/32]}\right)^{1-n} \\ &+ 4\sum_{i=1}^{8}\left(1+\frac{H/2+y}{a\cos[(2i-1)\pi/32]}\right)^{1-n} \\ &+ 2\sum_{i=1}^{7}\left(1+\frac{H/2-y}{a\cos[i\pi/16]}\right)^{1-n} \\ &+ 2\sum_{i=1}^{7}\left(1+\frac{H/2+y}{a\cos[i\pi/16]}\right)^{1-n}\Bigg],\end{aligned} \tag{12}$$

which is the normalized effective MFP based on the power-law distribution function. It is evaluated using the rarefaction parameter Kn, as a is dependent on the unconfined mean free path. For thermal cases the expression requires a_T.

From Eq. (12), it is easy to see that our PL model satisfies the physically intuitive requirements for $Kn \to 0$, i.e.

$$\beta_{\mathrm{PL}}\,|_{wall} \;\approx\; 1/2, \text{ and } \beta_{\mathrm{PL}}\,|_{bulk} \;\approx\; 1. \tag{13}$$

It is interesting to note that the phenomenological viscosity model derived by Fichman and Hetsroni [23], which also considered KL effects, gives an effective transport property value at the wall that is half its bulk value.

2.2 Comparison with Molecular Dynamics simulations

The β-function of Eq. (12) is now compared with MD simulation results [15] and the classical exponential probability function models of Stops [11] and Arlemark *et al.* [13], for both single- and parallel-wall cases. Single-wall results are deduced by assuming that the second wall is located an infinite distance from the first. In the case of parallel walls, KL overlap becomes apparent as Kn increases. Arlemark and Reese [15] carried out MD simulations using 50520 Lennard-Jones molecules, which yielded results that are within 1% accuracy. All simulations were carried out assuming a planar smooth bounding surface.

Figure 4a shows the variation of normalized effective MFP profiles (i.e. β) with normalized wall distance, y/λ. Our PL model predictions are in close agreement with MD simulations, although minor overpredictions are noticed in the bulk region. The PL model has a sharp gradient close to the wall, while both of the previous exponential-based models have shallower gradients and underpredict the MFP values in the wall vicinity. All three theoretical models converge to a similar value in the bulk region, as expected.

Results for the normalized MFP between two parallel surfaces are presented in Fig. 4b. MD simulation results for planar smooth surfaces are compared with both PL and exponential distribution-based models for various Kn in the transition regime. At $Kn = 0.2$, which is just beyond the slip-flow regime, the PL model is in fair agreement with the MD data in the near-wall region, but deviates slightly in the bulk region. The two exponential based models underpredict in the KL, but Arlemark *et al.* [13] achieve good agreement with the MD data in the bulk region. As the value of Kn increases, and the flow becomes increasingly rarefied, the classical models fail to predict the effective MFP in the wall region, or in the bulk. Both classical models underpredict the effective MFP values, although the Arlemark *et al.* results are slightly above Stops'. Effective MFP values predicted by the PL model compare very well to the MD data for both $Kn = 0.5$ and 1, although it overpredicts for $Kn = 1$ in the bulk. By $Kn = 2$, when the Knudsen layers from each surface completely overlap each other, the PL model shows significant deviations from the simulation data and overpredicts in the near-wall region, although there is fair agreement in the bulk region. The MD data shows a relatively sharp gradient of effective MFP in the near-wall region, compared to the theoretical predictions.

3 A new way of modeling rarefied gas flows

3.1 Isothermal pressure-driven gas flows

To test the merits of our PL-based effective MFP scaling, we further first consider isothermal pressure-driven gas flow along a planar-wall channel with walls a distance H apart, as depicted in Fig. 2. The channel height H is assumed to be much smaller than the channel width, so that the fluid essentially sees two infinite parallel plates separated by H, at coordinates $y = \pm H/2$. The flow is assumed to be fully hydrodynamically developed and two-dimensional, isothermal, laminar and steady, with a low Reynolds number (Re) so that inertial effects may be neglected.

With these assumptions, the governing equation is:

$$0 = -\frac{\partial P}{\partial x} - \frac{\partial \tau}{\partial y}, \tag{14}$$

where x is the streamwise coordinate, y the wall-normal coordinate, P the pressure and τ the stress, which is given as:

$$\tau = -\mu\left[\nabla \mathbf{U} + (\nabla \mathbf{U})^{tr}\right] + \left(\frac{2}{3}\mu - \kappa\right)(\nabla.\mathbf{U})I, \tag{15}$$

where μ is the fluid dynamic viscosity, κ the bulk viscosity, I the identity tensor and tr the transpose operator.

In Eq. (15) we can neglect volume dilation effects for rarefied gases [24]. From the kinetic theory of gases, the fluid viscosity can be explained in terms of the collisions between gas molecules, and of the free paths which the molecules describe between collisions. The collision time, or equivalently the free flight path between two successive collisions of a gas molecule, is closely related to the momentum exchange. The unconfined MFP is related to the shear viscosity [25]:

$$\mu = \rho \frac{\lambda}{\sqrt{\pi/2RT}}, \tag{16}$$

where R is the specific gas constant and T the gas temperature.

Equation (16) is assumed to be valid only for flows that are quasi-equilibrium. As discussed in section 2, within the KL the flight paths of gas molecules are affected by the presence of a solid wall. Using Eqs. (12) and (16) we can therefore posit a non-linear stress/strain-rate relation:

$$\tau = -\underbrace{\mu\beta_{\mathrm{PL}}}_{\mu_{\mathrm{eff(PL)}}} \frac{\partial U_x}{\partial y}, \tag{17}$$

where U_x is the fluid velocity in the axial direction.

Using Eq. (17) in Eq. (14) results in the following governing equation:

$$\mu \frac{\partial}{\partial y}\left(\beta_{\mathrm{PL}} \frac{\partial U_x}{\partial y}\right) = \frac{\partial P}{\partial x}. \tag{18}$$

This needs to be solved in conjunction with an appropriate slip boundary condition to capture the non-equilibrium phenomena in the slip and transition flow regimes.

The first-order slip boundary condition proposed by Maxwell [1] fails to predict the Knudsen-minimum in the mass flow rate [26], and researchers have consequently proposed higher-order slip models for a wide-range of Knudsen numbers. A review of a number of these higher-order slip models can be found in Reese and Zhang [27]. Deissler [28] derived a second-order slip boundary condition based on the concept of MFP for momentum and energy transfer, which can be expressed in its generalized form as:

$$U_{slip} = -C_1\lambda\left(\frac{\partial U_x}{\partial y}\right)_w - C_2\lambda^2\left(\frac{\partial^2 U_x}{\partial y^2}\right)_w, \qquad (19)$$

where U_{slip} is the slip velocity at the fluid-surface interface, and w indicates a quantity evaluated at the surface. While there is no general consensus on the slip coefficients C_1 and C_2, C_1 is set to ~ 1 by many authors and C_2 has a wide range from -0.5 to $5\pi/12$ [27]. Cercignani [29] proposed C_2 to be 0.9756 from kinetic theory considerations, and Hadjiconstantinou [30] corrected C_2 to 0.31.

It is important to note that Maxwell [1] and Deissler [28] derived first- and second-order slip boundary conditions assuming that the MFP is constant in the wall-adjacent gas layer. Guo *et al.* [10] proposed the following heuristic slip boundary condition to take into account the KL correction:

$$U_{slip} = -C_1\left(\lambda_{\text{eff}}\frac{\partial U_x}{\partial y}\right)_w - C_2\left[\lambda_{\text{eff}}\frac{\partial}{\partial y}\left(\lambda_{\text{eff}}\frac{\partial U_x}{\partial y}\right)\right]_w. \qquad (20)$$

This simply reduces to the conventional second-order slip boundary condition (19) if there is no KL, i.e. if $\lambda_{\text{eff}} = const$. In the present analysis, we implement this second-order slip boundary condition, and use $\lambda_{\text{eff(PL)}}$ given by Eq. (12). Values of C_1 and C_2 are chosen as 1 and 0.31 [30] respectively for the results reported below.

3.1.1 Solution procedure

We require results for the flow velocity profile across the channel, and some integral flow parameters, through solution of the governing equation with the slip boundary condition discussed above. In addition to the governing Eq. (18) and slip boundary condition (20), the ideal gas law is

$$P = \rho RT, \qquad (21)$$

and the Knudsen number is defined as

$$Kn = \frac{\lambda}{H}. \qquad (22)$$

The wall-normal coordinate, y, is normalized by H, and the axial velocity, U_x, by the free-molecular velocity $U_0 = -2H(\partial P/\partial x)/(\rho\sqrt{2RT})$ [31]. Using Eqs. (16) and (12), Eq. (18) in normalized form (indicated by $*$) is

$$\frac{\partial}{\partial y^*}\left(\beta_{\text{PL}}\frac{\partial U^*}{\partial y^*}\right) = -\frac{\sqrt{\pi}}{2Kn}, \qquad (23)$$

and Eq. (20) in normalized form is

$$(U^*)_{slip} = -C_1 Kn\left(\beta_{\text{PL}}\frac{\partial U^*}{\partial y^*}\right)_w - C_2 Kn^2\left[\beta_{\text{PL}}\frac{\partial}{\partial y^*}\left(\beta_{\text{PL}}\frac{\partial U^*}{\partial y^*}\right)\right]_w. \qquad (24)$$

Equation (23) is numerically solved for the normalized axial velocity profiles U^* by applying the slip boundary condition (24) at the upper wall ($y^* = 0.5$) and a symmetry condition at the centre of the channel ($y^* = 0$).

The solution of the conventional Navier-Stokes (NS) equations, with constant viscosity and first-order velocity slip, and using the unconfined MFP, is:

$$U^* = \frac{\sqrt{\pi}}{16Kn}\left[1 - 4(y^*)^2 + 4C_1 Kn\right], \qquad (25)$$

while the NS solution with second-order velocity slip using the unconfined MFP, is:

$$U^* = \frac{\sqrt{\pi}}{16Kn}\left[1 - 4(y^*)^2 + 4C_1 Kn + 8C_2 Kn^2\right]. \qquad (26)$$

The normalized mass flow rate G is in all cases

$$G = \frac{2\int_0^{H/2}\rho U_x dy}{\rho U_o H} = \int_0^{0.5} U^* dy^*. \qquad (27)$$

3.1.2 Results

In what follows, the *PL model* is the modified governing equation (23), with the use of effective MFP (12) and the second-order slip boundary condition (24). The cross-sectional velocity profiles of pressure-driven Poiseuille flow over a range of Knudsen numbers are presented in Fig. 5. Our PL model is compared with a Boltzmann solution [31] and with three hydrodynamic models: conventional first- (Eq. 25) and second-order (Eq. 26) slip models, and the R26 equations [32]. At $Kn = 0.113$, which is just beyond the slip-flow regime, the four hydrodynamic models predict similar values of slip velocity at the wall and all are close to the solution obtained from the Boltzmann equation. The conventional NS equations with both first- and second-order slip boundary conditions significantly underpredict the velocity in the bulk region. Our PL model and the R26 equations are in fair agreement with the Boltzmann solution, although the

PL model slightly underpredicts, and the R26 equations overpredict, the maximum velocity. At $Kn = 0.226$, the NS equations with slip boundary conditions overpredict the slip velocity and underpredict the maximum velocity at the centre. The second-order slip solution lies above the first-order slip results. Both our PL model and the R26 equations compare well with the solution obtained from the Boltzmann equation, however, the R26 equations show minor deviations in the wall-slip velocity. At higher Kn, the flow enters the transition regime and the non-equilibrium regions from each of the parallel walls start to overlap each other. Hence, the first-order slip model is solved only up to $Kn = 0.226$, and the second-order slip model up to $Kn = 1.128$. At $Kn = 0.451$ and $Kn = 0.677$, the PL model and R26 equations compare reasonably well with the Boltzmann solutions, although the R26 equations overpredict the slip velocity. At $Kn = 1.128$, deviations from the Boltzmann predictions are relatively less for our PL model than for the R26 equations.

Predictions of normalized slip velocity $(U^*)_{slip}$ are presented as a function of Kn in Fig. 6, and compared to Boltzmann simulation data [31]. First-order slip is a constant, and higher than the Boltzmann result for $Kn < 1$ and lower for $Kn > 1$. The second-order NS slip is too high, particularly at large Knudsen numbers. Our PL model and the R26 equations agree well with the Boltzmann solution up to $Kn \simeq 0.5$. Both models overpredict the wall-slip velocity for $Kn > 0.5$, though the deviations are relatively less with the PL model.

It is evident from Figs. 4 and 5 that in the transition regime, non-equilibrium effects are no longer limited to the wall-adjacent layer, but prevail in the bulk flow due to the overlap of Knudsen layers. Hence, simply using a higher-order slip model with modified slip coefficients may result in good wall slip-velocity results but will not improve the overall predictive capabilities of the NS equations into the transition regime. The accurate prediction of integral flow parameters in micro/nano-conduits is important in engineering MEMS devices. To obtain the integral flow parameters correctly, it is essential that field variables such as MFP and cross-sectional velocities are correct. However, it is important to note that the accurate prediction of integral flow parameters does not inturn guarantee that all the field variables are predicted accurately.

Figure 7 shows the variation of normalized flow rate G with inverse Knudsen number, $\delta_m = \sqrt{\pi}/(2Kn)$. In Fig. 7a, our PL model results are compared with experimental data [33], BGK simulation data [34] and the NS equations with Stops' MFP model and the second-order slip condition (24). In the slip flow regime, both the PL model and Stops' model agree reasonably well with the experimental data and the BGK simulation results. However, around $\delta_m \sim 1$, Stops' MFP based slip model starts to significantly underpredict the flow rate, whilst our PL model follows the BGK simulation data reasonably well until Kn reaches about 10.

Flow rate results of our PL model with $n = 3$ are shown in Fig. 7b to compare with the exact Boltzmann solution [31], DSMC data [35], R26 results [32], NS equations with first- and second-order slip, and our PL model with first-order slip. Here the first-order slip for the PL model results are obtained simply by setting $C_2 = 0$. For $Kn > 0.1$, which is just beyond the slip flow regime, the NS equations with first-order slip underpredict the flow rate, although the other hydrodynamic models are in good agreement with the Boltzmann and DSMC data up to $Kn \sim 0.2$. The NS results with second-order slip are good up to $Kn \sim 0.5$, but significantly overpredict beyond that. The R26 equations show good agreement until $Kn \sim 2$. But our PL model with second-order slip follows the Boltzmann results up to $Kn \sim 10$. Both PL and NS models with first-order slip fail to predict the Knudsen minimum. The other three hydrodynamic models show a Knudsen minimum; however, the NS equations with second-order slip predict the minimum at a value of Kn smaller than that predicted by the Boltzmann equation.

3.2 Thermal transpiration

To further test the applicability of our PL-based effective MFP scaling, we consider thermal transpiration of a rarefied gas along a planar-wall channel with walls a distance H apart. We consider the steady-state situation of a closed-ended channel with insulated sidewalls, filled with a single-component rarefied gas. The channel ends are maintained at different uniform temperatures. Reynolds' [36] experimental and Maxwell's [1] independent theoretical studies were the first to describe the phenomenon of thermal transpiration (creep), where the fluid starts moving in the direction from a cold region towards a hot region. Due to this flow, a pressure difference between the hot and cold ends of the capillary will be established, and a pressure return flow will occur that will partially or completely balance the thermal creep flow. The physical explanation of thermal creep has been presented by Sone [3].

3.2.1 Solution procedure

The flow is assumed to be fully hydrodynamically developed and two-dimensional, laminar and steady, i.e. zero net mass flow, with a low Reynolds number (Re) so that inertial effects may be neglected.

With these assumptions, the governing equations are:

$$0 = -\frac{\partial P}{\partial x} - \frac{\partial \tau}{\partial y}, \tag{28}$$

and

$$0 = -\frac{\partial q}{\partial x}, \tag{29}$$

where q is the heat flux, which is given as:

$$q = -k\frac{\partial T}{\partial x}, \tag{30}$$

where k is the thermal conductivity, defined as [25]:

$$k = \rho C_p \frac{\lambda_T}{\sqrt{\pi/2RT}}. \tag{31}$$

Using the non-dimensional effective MFP for a thermal case, $\beta_{\mathrm{PL(T)}}$, we therefore posit a non-linear constitutive relation for heat flux:

$$q = -k\beta_{\mathrm{PL(T)}} \frac{\partial T}{\partial x}. \tag{32}$$

Equations (28), (29) and (32) are solved in conjunction with the following slip boundary condition:

$$U_{slip} = \underbrace{-C_1 \left(\lambda_{\mathrm{eff}} \frac{\partial U_x}{\partial y}\right)_w - C_2 \left[\lambda_{\mathrm{eff(T)}} \frac{\partial}{\partial y}\left(\lambda_{\mathrm{eff(T)}} \frac{\partial U_x}{\partial y}\right)\right]_w}_{U_{Pslip}} + \underbrace{\frac{3}{4} \frac{k\beta_{\mathrm{PL(T)}}}{C_v \rho T} \left(\frac{\partial T}{\partial x}\right)_w}_{U_{Tslip}}, \tag{33}$$

where U_{Pslip} and U_{Tslip} are the isothermal and thermal creep components of the slip velocity. This boundary condition simply reduces to the conventional slip condition if there is no KL, i.e. if $\lambda_{\mathrm{eff}} = const$.

The wall-normal coordinate, y, is normalized by H, i.e. $y^* = y/H$ and the axial velocity components, U_T, the thermal creep velocity and U_P, the Poiseuille velocity, by the free-molecular velocities $U_{T0} = \sqrt{2RT}(H/T)(\partial T/\partial x)$ and $U_{P0} = -2H(\partial P/\partial x)/(\rho\sqrt{2RT})$. Using Eqs. (16, 31, 12 and 18) we solve for the normalized velocity components (U_T^*, U_P^*), normalized flow rate components ($G_T = 2\int_0^{0.5} U_T^* dy^*$, $G_P = 2\int_0^{0.5} U_P^* dy^*$), and thermo molecular pressure difference (TMPD) i.e. $(T/P)(dP/dx)/(dT/dx)$, with the assumption of zero net mass flow rate at steady state.

3.2.2 Results

The thermal creep components of the cross-sectional velocity profiles over a range of Knudsen numbers are presented in Fig. (8). Our PL model for this thermal case is validated against a Boltzmann solution [31] and compared with two hydrodynamic models: a conventional slip solution, and the Arlemark *et al.* [13] exponential-based results. At $Kn = 0.2$, which is just beyond the slip-flow regime, the PL MFP model predicts a wall-slip velocity close to the solution obtained from the Boltzmann equation, and displays minor deviations in the KL. The exponential MFP model produces shallower gradients in the KL, compared to the PL model, and underpredicts the velocities in the bulk flow region. The conventional NS equations with second-order slip boundary conditions overpredict in both the KL and bulk flow regions. At $Kn = 0.8$ and $Kn = 2.0$, which are in the transition regime, the exponential model overpredicts in both the Knudsen layer and the bulk flow. The PL model has fair agreement in the region close to the wall, with minor deviations in the bulk flow region. At even higher Kn, the non-equilibrium regions from each of the parallel walls start to overlap each other: the PL model underpredicts, and the exponential model overpredicts the results (not shown in this paper, see Dongari *et al.* [37]).

Figure (9) shows the variations of the thermal creep and Poiseuille components of the normalized flow rates (G_T and G_P) with Knudsen number. Our PL model results are compared with hard sphere Boltzmann results [38], BGK simulation data [34], the NSF equations using the exponential MFP model, and a conventional 2nd order slip solution. The classical slip solution has fair agreement up to the slip flow regime, but diverges with further increase in Kn. The exponential MFP model predicts good results up to $Kn \sim 0.5$ in the case of the thermal creep component and up to $Kn \sim 2$ for the Poiseuille component, but overpredicts and underpredicts for higher Kn, respectively. The PL model is in fair agreement with the hard sphere data up to $Kn \sim 10$, with minor underpredictions for both G_T and G_P.

Figure (9) also shows the TMPD variation with Knudsen number. This parameter is of great interest in micro/nano machine engineering, as it describes the maximum pressure difference that a thermal creep pump can produce for a given temperature difference applied across the channel ends. The BGK simulation underpredicts throughout the Kn regime, which may be due to the limitations of the BGK model when applied to non-isothermal flow cases.

4 Conclusions

We have developed new power-law probability distribution function for the free-paths of gas molecules in order to better describe non-equilibrium particularly flow physics, in the Knudsen layer. This power-law model for mean free path has been validated against MD simulation data, and compared with other existing theoretical models. A simple constitutive scaling approach to model the Knudsen layer flow within a conventional continuum fluid dynamics framework has also been described. This was tested for the cases of isothermal pressure-driven gas flow and thermal transpiration of a rarefied gas in micro/nano channels.

In general, our new power-law MFP model is more accurate than the conventional model in capturing many non-equilibrium effects in the transition regime. Our results for both isothermal and thermal creep flows indicate that it provides a reasonable description of the nonlinear flow characteristics in the Knudsen layer up to $Kn \sim O(1)$. In predicting integral flow parameters, such as normalized flow rate and the TMPD, the power-law model provides a significant improvement up to $Kn \sim 5$. The classical exponential probability distribution function MFP models provide accurate results in the Knudsen layer only up to $Kn \sim 0.2$, and integral flow parameter results are reasonable up to $Kn \sim 1$.

The NSF equations with higher-order slip boundary conditions can correctly capture the surface slip by tuning the slip coefficients, but do not necessarily then provide accurate

velocity profiles in both the Knudsen layer and the bulk flow regions. While the NSF equations with an exponential-based MFP can provide good velocity profiles in the Knudsen layer up to the early transition regime, with the new power-law model we can also adjust the velocity profile at a fixed Knudsen number by using the exponent n.

The advantage of the power-law MFP constitutive scaling technique is that it is based on simple physical arguments, and it can easily be implemented in conventional CFD codes in order to capture some of the trends associated with the complex non-equilibrium physics of the Knudsen layer.

While it is important not to draw strong conclusions based on just two test cases, the present results may motivate future work into understanding the origin of non-equilibrium physics in rarefied gases, including:
(i) whether the power-law behaviour is appropriate for rarefied gases in complex geometries, with specular-diffusive and explicit rough walls, and also for non-isothermal cases;
(ii) developing a separate non-exponential distribution function to describe the thermal Knudsen layer (in particular, in order to predict the bimodality in the cross sectional temperature profile);
(iii) revisiting higher-order velocity slip and temperature jump boundary conditions, that are conventionally derived under the assumption of constant MFP in Knudsen layers, using geometry-dependent effective MFP models.

Acknowledgments

The research leading to these results has received funding from the European Community's Seventh Framework Programme FP7/2007-2013 under grant agreement ITN GASMEMS n^o 215504. JMR would like to thank the Royal Academy of Engineering and the Leverhulme Trust for support through a Senior Research Fellowship. JMR would also like to thank the President and Fellows of Magdalen College, Oxford, for support through a Visiting Fellowship.

References

[1] Maxwell, J. C., 1879. "On stresses in rarefied gases arising from inequalities of temperature". *Philos. Trans. Roy. Soc. Part 1,* **170**, pp. 231–256.

[2] Lockerby, D. A., Reese, J. M., and Gallis, M. A., 2005. "The usefulness of higher-order constitutive relations for describing the knudsen layer". *Phys. Fluids,* **17**, 100609.

[3] Sone, Y., 2002. *Kinetic Theory and Fluid Dynamics*. Birkhauser, Boston.

[4] Bird, G. A., 1994. *Molecular Gas Dynamics and the Direct Simulation of Gas Flows*. Oxford University Press, New York.

[5] Cercignani, C., Frangi, A., Lorenzani, S., and Vigna, B., 2007. "Bem approaches and simplified kinetic models for the analysis of damping in deformable mems". *Eng. Anal. Boundary Elem.,* **31**, pp. 451–457.

[6] Lockerby, D. A., Reese, J. M., and Gallis, M. A., 2005. "Capturing the Knudsen layer in continuum-fluid models of non-equilibrium gas flows". *AIAA J.,* **43**, pp. 1391–1393.

[7] Lilley, C. R., and Sader, J. E., 2007. "Velocity gradient singulary and structure of the velocity profile in the knudsen layer according to the Boltzmann equation". *Phys. Rev. E,* **76**, 026315.

[8] Lockerby, D. A., and Reese, J. M., 2008. "On the modelling of isothermal gas flows at the microscale". *J. Fluid Mech.,* **604**, pp. 235–261.

[9] Zhang, Y. H., Gu, X. J., Barber, R. W., and Emerson, D. R., 2006. "Capturing Knudsen layer phenomena using a lattice Boltzmann model". *Phys. Rev. E,* **74**, 046704.

[10] Guo, Z. L., Shi, B. C., and Zheng, C. G., 2007. "An extended Navier-Stokes formulation for gas flows in the Knudsen layer near a wall". *EPL,* **80**, pp. 24001–24006.

[11] Stops, D. W., 1970. "The mean free path of gas molecules in the transition regime". *J. Phys. D: App. Phys.,* **3**, pp. 685–696.

[12] Kennard, E. H., 1938. *Kinetic Theory of Gases with an Introduction to Statistical Mechanics*. McGraw-Hill, New York.

[13] Arlemark, E. J., Dadzie, S. K., and Reese, J. M., 2010. "An extension to the Navier-Stokes equations to incorporate gas molecular collisions with boundaries". *J. Heat Trans.,* **132**, 041006.

[14] Dongari, N., Zhang, Y. H., and Reese, J. M., 2011. "Molecular free path distribution in rarefied gases". *J. Phys. D: Appl. Phys.,* **44**, 125502.

[15] Arlemark, E. J., and Reese, J. M., 2009. Investigating the effect of solid boundaries on the gas molecular mean-free-path. ASME ICNMM2009-82080, Pohang, South Korea.

[16] Einstein, A., 1956. *Investigations on the Theory of Brownian Movement*. Dover, New York.

[17] del Castillo-Negrete, D., Carreras, B. A., and Lynch, V. E., 2005. "Nondiffusive transport in plasma turbulence: a fractional diffusion approach". *Phys. Rev. Lett.,* **94**, 065003.

[18] Scharfe, M. E., 1970. "Transient photoconductivity in vitreous as2se3". *Phys. Rev. B,* **2**, pp. 5052–5034.

[19] Benisti, D., and Escande, D. F., 1998. "Nonstandard diffusion properties of the standard map". *Phys. Rev. Lett.,* **80**, 4781.

[20] Montroll, E. W., and Scher, H., 1973. "Random walks on lattices. iv. continuous-time walks and influence of absorbing boundaries". *J. Stat. Phys.,* **9**, pp. 101–135.

[21] Cercignani, C., 1990. *Mathematical Methods in Kinetic Theory*. Plenum Press, New York.

[22] Grolimund, D., Borkovec, M., Federer, P., and Sticher, H., 1995. "Measurement of sorption isotherms with flow-through reactors". *Environ. Sci. Techno.,* **29**, pp. 2317–2321.

[23] Fichman, M., and Hetsroni, G., 2005. "Viscosity and slip velocity in gas flow in microchannelss". *Phys. Fluids,* **17**, 123102.

[24] Bird, R. B., Stewart, W. E., and Lightfoot, E. N., 1960.

Transport Phenomena. John Wiley and Sons, New York.

[25] Cercignani, C., 1988. *The Boltzmann Equation and its Applications*. Springer-Verlag, New York.

[26] Dongari, N., Agrawal, A., and Agrawal, A., 2007. "Analytical solution of gaseous slip flow in long microchannels". *Int. J. Heat Mass Trans.,* **50**, pp. 3411–3421.

[27] Reese, J. M., and Zhang, Y. H., 2009. "Simulating fluid flows in micro and nano devices: the challenge of non-equilibrium behaviour". *J. Comp. Theor. Nanosci.,* **14**, pp. 2061–2074.

[28] Deissler, R. G., 1964. "An analysis of second-order slip flow and temperature jump boundary conditions for rarefied gases". *Int. J. Heat Mass Trans.,* **7**, pp. 681–694.

[29] Cercignani, C., 1964. Higher order slip according to the linearized Boltzmann equation. Institute of Engineering Research Report AS-64-19, University of California, Berkeley.

[30] Hadjiconstantinou, N. G., 2003. "Comment on Cercignani's second-order slip coefficient". *Phys. Fluids,* **15**, pp. 2352–2355.

[31] Ohwada, T., Sone, Y., and Aoki, K., 1989. "Numerical analysis of the poiseuille and thermal transpiration flows between parallel plates on the basis of the Boltzmann equation for hard-sphere molecules". *Phys. Fluids A,* **1**, pp. 2042–2049.

[32] Gu, X.-J., and Emerson, D. R., 2009. "A high-order moment approach for capturing non-equilibrium phenomena in the transition regime". *J. Fluid Mech.,* **636**, pp. 177–226.

[33] Ewart, T., Perrier, P., Graur, I. A., and Meolans, J. B., 2007. "Mass flow rate measurements in a microchannel, from hydrodynamic to near free molecular regimes". *J. Fluid Mech.,* **584**, pp. 337–356.

[34] Loyalka, S. K., 1975. "Kinetic theory of thermal transpiration and mechanocaloric effects". *J. Chem. Phys.,* **63**, pp. 4054–4560.

[35] Hadjiconstantinou, N. G., 2006. "The limits of Navier-Stokes theory and kinetic extensions for describing small scale gaseous hydrodynamics". *Phys. Fluids,* **18**, 111301.

[36] Reynolds, O., 1880. "On certain dimensional properties of matter in the gaseous state". *Phil. Trans. R. Soc. B,* **170**, pp. 727–845.

[37] Dongari, N., Zhang, Y. H., and Reese, J. M., 2010. "Power-law free path distribution function for thermal transpiration". *Proceedings of the 2nd GASMEMS Workshop, Les Embiez, France*, GASMEMS2010-DY06.

[38] Sharipov, F., and Bertoldo, G., 2009. "Poiseuille flow and thermal creep based on the boltzmann equation with the lennard-jones potential over a wide range of the knudsen number". *Phys. Fluids,* **21**, 067101.

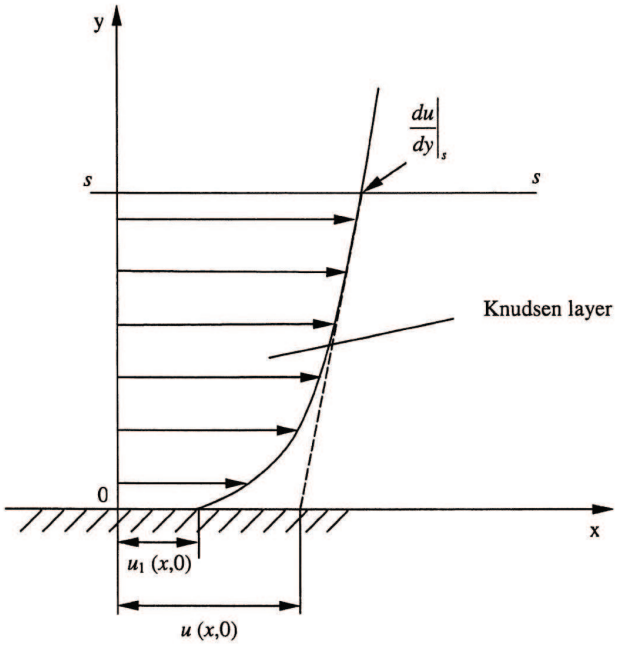

Fig. 1. Schematic of the momentum Knudsen layer (KL) close to a planar wall, showing the microscopic slip $u_1(x,0)$; the macroscopic slip $u(x,0)$ is required when using the classical Navier-Stokes equations with a slip boundary condition. Here s denotes the plane, at the outer edge of the KL.

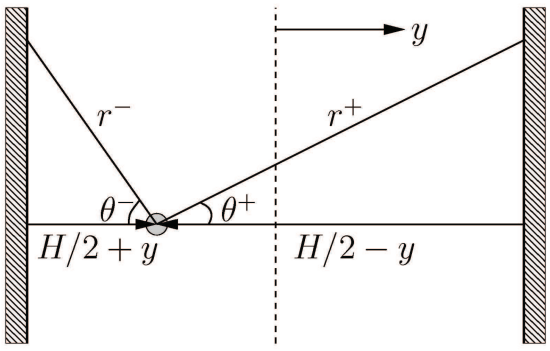

Fig. 2. A molecule confined between two planar walls with spacing H. The molecule has an equal probability to travel in any zenith angle θ^- or θ^+ or to travel in either the positive or negative y-direction. The molecule under consideration is assumed to have just experienced an intermolecular collision at its current position $H/2+y$.

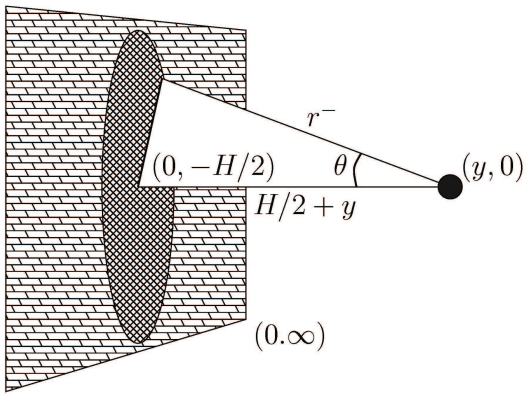

Fig. 3. A molecule at a distance $H/2+y$ from a planar wall; possible trajectories for travelling in the negative y-direction in cylindrical coordinates $[H/2+y,(H/2+y)\tan\theta]$.

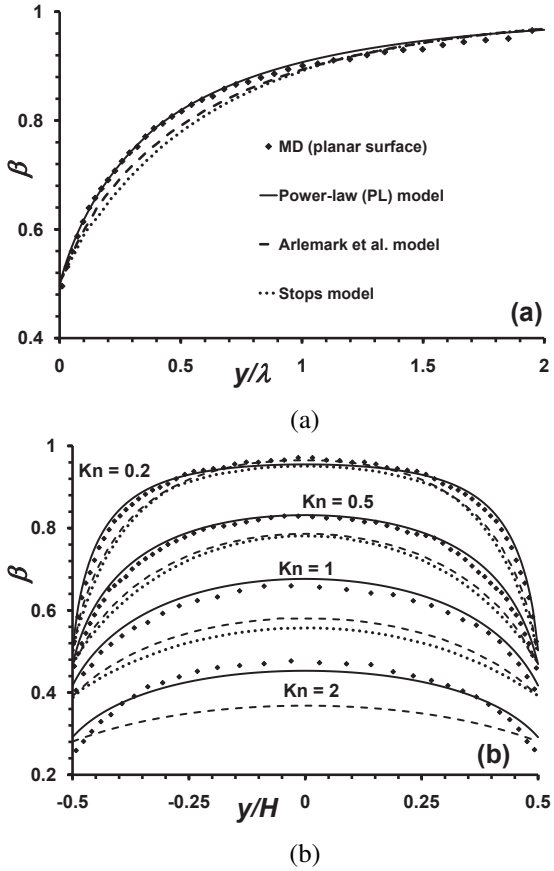

Fig. 4. Variation of normalized mean free path, β, with normalized distance from a surface; (a) single-wall case and (b) parallel-wall case. Comparison of our power-law (PL) model with molecular dynamics (MD) simulation data [14], and Arlemark *et al.* [13] and Stops [11] exponential models, for various Knudsen numbers.

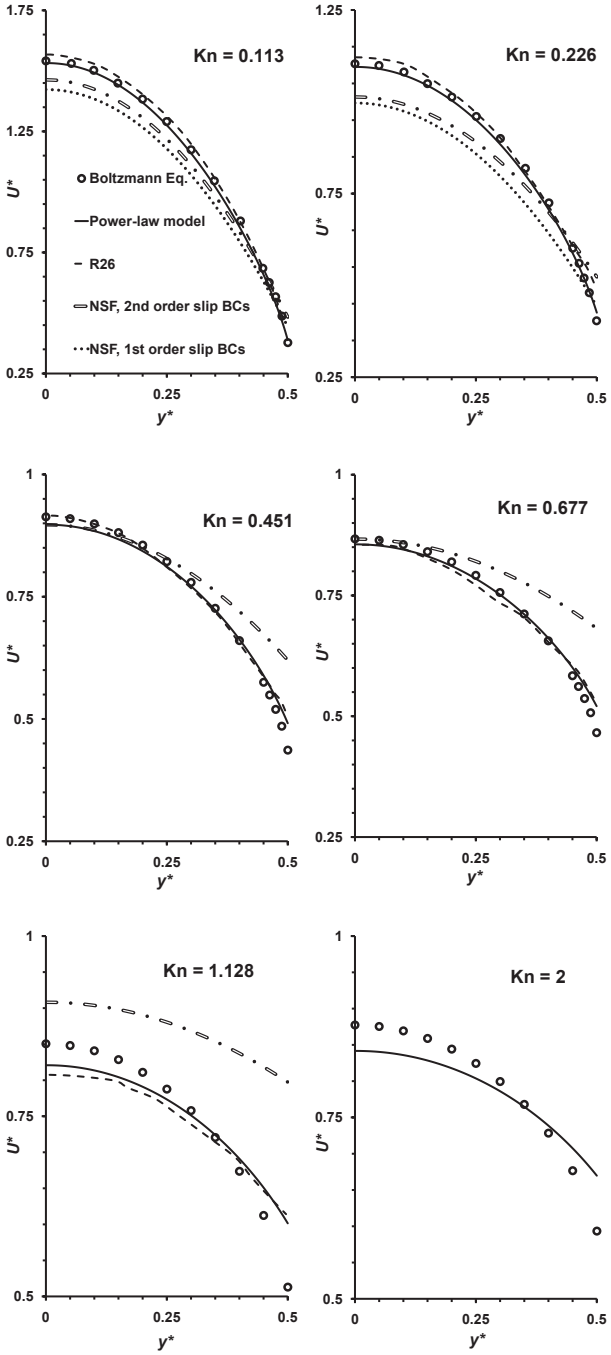

Fig. 5. Normalized half cross-channel velocity profiles for various Knudsen numbers. Comparison of our power-law (PL) model results with the solution of the Boltzmann equation [31], R26 moment equations [32], and conventional NS equations with first- and second-order slip.

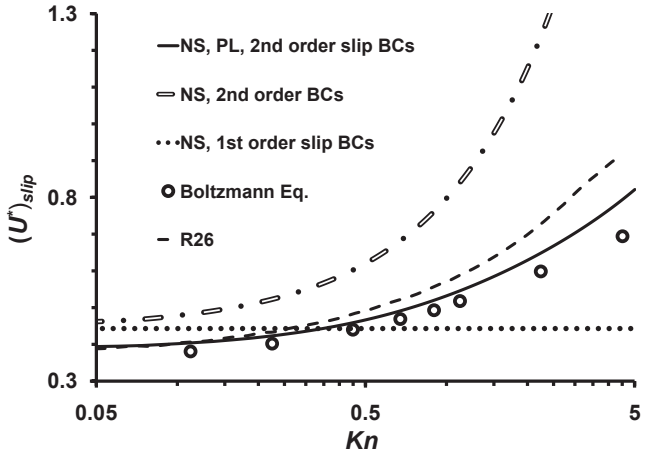

Fig. 6. Variation of normalized slip velocity with Knudsen number, comparison of power-law (PL) model with the solution of the Boltzmann equation [31], R26 moment equations [32], and the conventional NS equations with first- and second-order slip.

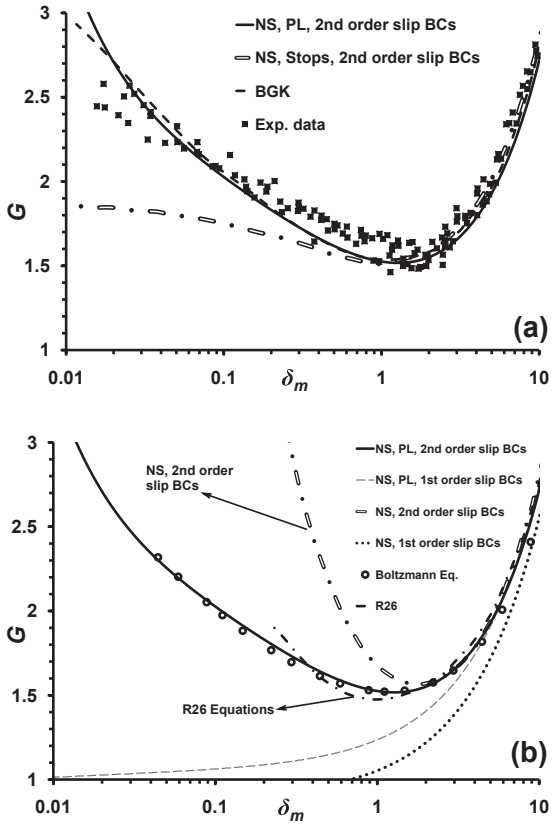

Fig. 7. Normalized mass flow rate (G) variation with inverse Knudsen number (δ_m). Comparison of power-law (PL) model results with: (a) experimental data [33] and BGK simulation results [34]; (b) the solution of the Boltzmann equation (- -) [31], R26 moment equations (-··-) [32] and the conventional NS equations with first- and second-order slip.

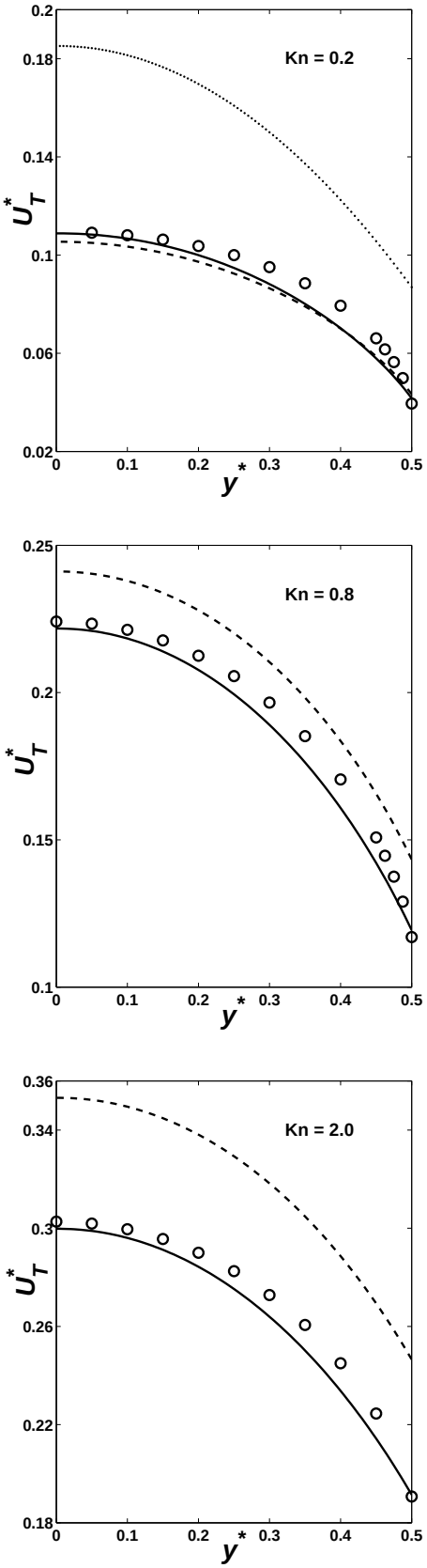

Fig. 8. Normalized thermal creep component of half cross-channel velocity profiles for various Knudsen numbers. Comparison of our power-law (PL) model results (thick line) with the solution of the Boltzmann equation (symbols, Ohwada *et al.* [31]), exponential MFP model (dashed line, Arlemark *et al.* [13]), and the conventional slip solution (dotted line).

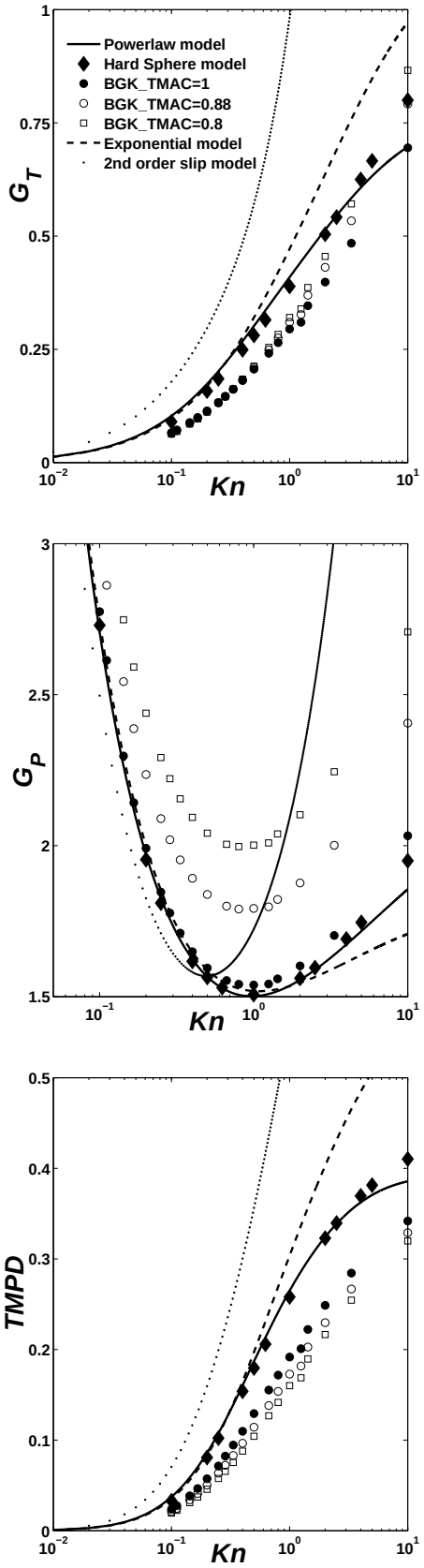

Fig. 9. Variation of normalized thermal creep component (G_T) and Poiseuille component (G_P) of flow rates, and TMPD, with Knudsen number (Kn). Comparison of our power-law (PL) model results with: hard sphere Boltzmann equation [38], BGK simulation data [34], exponential MFP model [13], and the conventional 2nd order slip solution.